AbINS: The modern software for INS interpretation

Krzysztof Dymkowski, Stewart F. Parker, Felix Fernandez-Alonso and Sanghamitra Mukhopadhyay

Published version information

Citation: K Dymkowski et al. "AbINS: The modern software for INS interpretation. Physica B, vol. 551 (2018): 443-448.

DOI: 10.1016/j.physb.2018.02.034

Accepted Manuscript

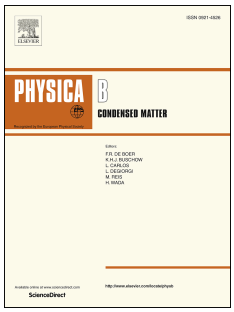

AbINS: The modern software for INS interpretation

Krzysztof Dymkowski, Stewart F. Parker, Felix Fernandez-Alonso, Sanghamitra Mukhopadhyay

PII: S0921-4526(18)30154-6

DOI: 10.1016/j.physb.2018.02.034

Reference: PHYSB 310751

To appear in: *Physica B: Physics of Condensed Matter*

Received Date: 29 August 2017

Revised Date: 20 February 2018

Accepted Date: 21 February 2018

Please cite this article as: K. Dymkowski, S.F. Parker, F. Fernandez-Alonso, S. Mukhopadhyay, AbINS: The modern software for INS interpretation, *Physica B: Physics of Condensed Matter* (2018), doi: 10.1016/j.physb.2018.02.034.

AbINS: the modern software for INS interpretation

Krzysztof Dymkowski[a], Stewart F. Parker[b], Felix Fernandez-Alonso[b,c], Sanghamitra Mukhopadhyay[b,d,*]

[a]*Scientific Computing Department, Rutherford Appleton Laboratory, Chilton, Didcot, Oxfordshire OX11 0QX, United Kingdom*
[b] *ISIS Facility, Rutherford Appleton Laboratory, Chilton, Didcot, Oxfordshire OX11 0QX, United Kingdom*
[c] *Department of Physics and Astronomy, University College London, Gower Street, London WC1E 6BT, United Kingdom*
[d]*Department of Materials, Imperial College London, Exhibition Road, London SW7 2AZ, United Kingdom*

Abstract

Inelastic neutron scattering (INS) spectroscopy, contrary to other vibrational spectroscopic techniques such as infrared or Raman spectroscopies, provides much richer microscopic insight into a material due to the absence of selection rules induced by the system's symmetry and *via* its dependence on both energy (E) and momentum (**Q**) transfer. First-principles density functional theory (DFT) based calculations are now routinely used to interpret infrared and Raman spectra. These calculations can also be used to interpret INS spectra, however, the need to include the neutron scattering cross sections, overtones and combination modes, together with instrument specific E-**Q** windows make the data analysis challenging. Here we present AbINS: a new generation of software to interpret INS spectra using ab initio phonon data. AbINS is an open-source package implemented as a plugin to the neutron data analysis software, Mantid and offers the facility to plot the full (**Q**, E) map for powder samples, with the option to extract individual atomic contributions. This option is then applied to analyse the vibrational spectrum of non-hydrogenous K_2SiF_6 to extract atom-type contributions identifying T_{1g} librational mode of the $[SiF_6]^{2-}$ ion together with the T_{2u} F–Si–F bending mode.

Keywords: Inelastic Neutron Scattering, Vibrational spectroscopy, calculated INS, scientific software, computational simulations, K_2SiF_6.

1. Introduction

Inelastic neutron scattering (INS) provides a very special form of vibrational spectroscopy. Contrary to the widely used optical spectroscopies such as infared and Raman, in which the spectrum is obtained as a result of the interaction between photons and the electron density, in INS the neutron flux interacts with the nuclei themselves. This makes INS complementary in many ways to other spectroscopic techniques. Firstly, there are no selection rules in INS and, in principle, all transitions are observable. Furthermore, the INS signal is directly proportional to the amplitude of motion and the scattering cross section of the atoms involved in the mode.

Current progress in computational power, together with the optimization of DFT techniques, makes it possible to calculate vibrational or phonon spectra with high accuracy. These calculations can also be used to interpret INS spectra. AbINS is a new generation of software to interpret INS spectra using ab initio phonon data from DFT programs. It is an open-source package and can be used on Linux, Windows and MacOS. It is implemented as a plugin to the neutron data analysis software Mantid [1]. AbINS uses the phonon data calculated by DFT programs, such as CASTEP [2] and CRYSTAL [3], to generate the calculated INS spectrum of a powder sample, making it easier to establish a connection between computational results and experiments.

This document is organised as follows. First, in section 2 the main components of the theory of INS spectroscopy for both indirect geometry and direct geometry instruments are briefly presented and the approximation used for the powder averaging is outlined. In section 3, the capabilities of AbINS are presented. In section 4, examples of calculated spectrum along with the observed INS spectrum are presented. Conclusions and future work are presented in the last section.

*Corresponding author: Tel: +44(0)12358190
Email address: sanghamitra.mukhopadhyay@stfc.ac.uk (Sanghamitra Mukhopadhyay)

2. Theory

2.1. Inelastic neutron scattering

In the simplest scenario for inelastic neutron scattering, a neutron is scattered by one atom. Neutrons in the incident flux, characterized by $\mathbf{k}_i$ and frequency ν_i, can be described by the plane wave function:

$$\psi_i = Ae^{i(B-\nu_i t)}e^{i\mathbf{k}_i\mathbf{r}} \tag{1}$$

$\mathbf{k}_i$ defines the momentum of the neutron and $E_i = \nu_i h$ its energy. A and B are constants. After scattering, both the energy and momentum of the neutron are changed to $\mathbf{k}_f$ and $E_f = \nu_f h$ final energy. After scattering, the neutron can be described by:

$$\psi_f = Ae^{i(B-\nu_f t)}\frac{b}{\mathbf{r}}e^{i\mathbf{k}_f\mathbf{r}} \tag{2}$$

b is the *scattering length* and is both element and isotope specific. After scattering, the momentum transfer $\mathbf{Q}$ is given by:

$$\mathbf{Q} = \mathbf{k}_f - \mathbf{k}_i \tag{3}$$

and the energy transfer E by:

$$E = h(\nu_f - \nu_i) = hc(\omega_f - \omega_i) \tag{4}$$

where:

h –Planck constant

c – speed of light

ω_f, ω_i energies in cm^{-1}; index $_f$ corresponds to final energy and index $_i$ corresponds to incident energy

2.2. Scattering function

During an experiment many neutrons are scattered by a sample. The resultant scattering can be expressed by the *partial differential cross-section*. It is defined as the number of neutrons, with final energy between E' and $E' + dE$, scattered per second into a small solid angle $d\Omega$ divided by the incident flux Φ, which is the number of neutrons per unit area per second, the area being perpendicular to the direction of the neutron beam.

The partial differential cross-section is proportional to the *scattering function* (sometimes this quantity is also called the *scattering law*) $S(\mathbf{Q}, E)$:

$$\frac{d^2\sigma}{d\Omega dE'} = \frac{\mathbf{k}_f}{\mathbf{k}_i}S(\mathbf{Q}, E) \tag{5}$$

Where $S(\mathbf{Q}, E)$ has already included the scattering length.

2.3. Calculation of S(Q, E)

The general scheme of calculation is presented in figure 1. Using the atomic displacements and frequencies obtained from DFT vibrational or phonon calculations, one can calculate a *discrete S(Q,E)* using a semi-empirical powder averaging model [4]. In order to calculate a *theoretical S(Q,E)* to compare with experimental data, one has to evaluate the convolution of the discrete *S(Q, E)* with an experimental resolution function.

Within the semi-empirical powder averaging model [4], each phonon is treated as an independent quantum harmonic oscillator. Within this model, *S(Q, E)* which corresponds to the first order quantum events (the *fundamentals*) can be presented in the following way:

$$S^j(Q(\omega_i), \omega_i) = \frac{Q^2(\omega_i)\mathrm{Tr}[B_{\omega_i}]}{3}] \tag{6}$$
$$exp\left(-Q^2(\omega_i)\alpha^j_{\omega_i}\coth^2\left(\frac{\hbar\omega_i}{2k_BT}\right)\right)\sigma^j$$

$$\alpha^j_{\omega_i} = \frac{1}{5}\left\{\mathrm{Tr}[A^j] + \frac{2B^j_{\omega_i} : A^j}{\mathrm{Tr}[B^j_{\omega_i}]}\right\} \tag{7}$$

where:

$$B^j_{\omega_i} = c^j_{\omega_i}(c^j_{\omega_i})^T M^j\frac{C_2}{\omega_i}, \quad C_2 = \frac{\hbar}{4\pi}, \quad A^j = \textstyle\sum_i B^j_{\omega_i},$$

$$\beta^j = A^j/3$$

j is the atom index, ω_i is the ith normal mode in (cm^{-1}), M^j is the mass of jth atom, $c^j_{\omega_i}$ is the atomic displacement for the jth atom in the ith normal mode, Q is the momentum transfer (in $\mathrm{Å}^{-1}$), σ^j is the scattering cross section of the jth atom, C_1 is 2 if i=j and 1 otherwise and here, the operation : indicates the contraction of two tensors.

Analogously, *S(Q, E)* which corresponds to second quantum order events can be expressed as the following:

$$S^j(Q(\omega_{ik}), \omega_{ik}) = \frac{Q^4(\omega_{ik})}{15 * C_1} \tag{8}$$
$$\left(\mathrm{Tr}B^j_{\omega_i}\mathrm{Tr}B^j_{\omega_k} + B^j_{\omega_i} : B^j_{\omega_k} + B^j_{\omega_k} : B^j_{\omega_i}\right)$$
$$exp\left(-Q^2(\omega_{ik})\beta^j\coth^2\left(\frac{\hbar\omega_{ik}}{2k_BT}\right)\right)\sigma^j \tag{9}$$

Second quantum order events are overtones (0 to 2 transitions) and combinations (simultaneous transitions of two different harmonic oscillators).

Within AbINS, higher quantum order events up to 4th order have been implemented. Exact expressions can be

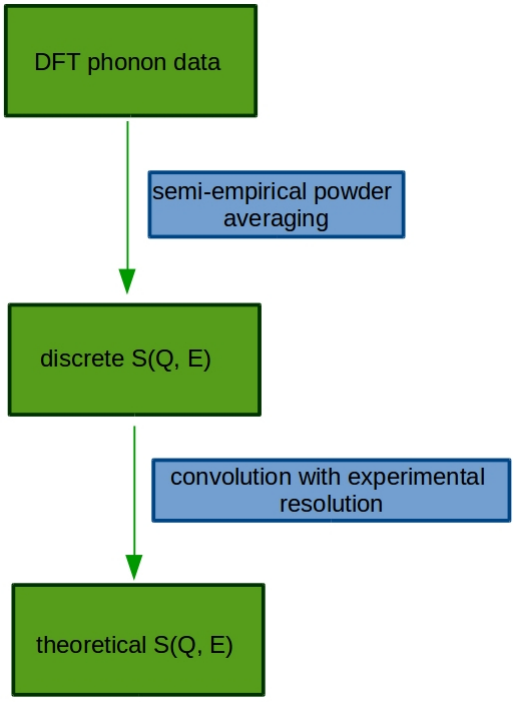

Figure 1: (Colour online) Schematic representation of the generation of the theoretical scattering function. from phonon DFT data, discrete values of *S(Q, E)* are then obtained by means of powder averaging. In order to compare the discrete *S(Q, E)* with experimental data, it is convolved with an experimental resolution function. The theoretical *S(Q, E)* may then be directly compared with experiment.

found in [4]. Q^2 is calculated from momentum conservation:

$$Q^2(\omega) = k_i^2(\omega) + k_f^2 - 2\sqrt{k_i^2(\omega)k_f^2}cos(\Theta) \tag{10}$$

where

Θ – scattering angle.

After evaluating equations (6) - (10), one obtains discrete *S(Q, E)* for each quantum order event and for each atom: $S_{discrete}$. In order to compare such a quantity with an experimental spectrum, it has to be convolved with an experimental resolution $f(\omega)$ to obtain the theoretical S^{nj}_{theory}:

$$S^{nj}_{theory}(Q,\omega) = S^{nj}_{discrete}(Q,\omega) * f(\omega) \tag{11}$$

2.4. Indirect geometry instruments

In the case of indirect geometry instruments, the final energy of the neutron is fixed and as a result:

$$k_i^2(\omega) = \frac{4\pi c(\omega + E_{final})m_n}{\hbar} \tag{12}$$

$$k_f^2 = \frac{4\pi c E_{final} m_n}{\hbar} \tag{13}$$

with energy transition ω (for the sake of simplicity, the index has been omitted) in cm^{-1}, E_{final} also in cm^{-1}, m_n as mass of neutron in *amu* and $\hbar/c$ is expressed in *amu* cm^{-1} Å^2 units ($\hbar/(4\pi c)$ = 16.8576 [amu cm^{-1} Å^2]). Θ is the scattering angle with respect to the initial neutron flux. In the case of TOSCA-like indirect geometry instruments only one angle Θ needs to be taken into account.

For indirect geometry instruments $f(\omega)$ has the following form:

$$f(\omega) = \frac{1.0}{\sqrt{2\sigma^2(\omega)\pi}} \exp\left(-\frac{1}{2}\frac{\omega^2}{\sigma^2(\omega)}\right) \tag{14}$$

where:

$$\sigma(\omega) = A\omega^2 + B\omega + C \tag{15}$$

with A, B, C as instrument dependent constants. The total *S(Q, E)* is a sum over all atomic contributions.

2.5. Direct geometry instruments

Implementation of the two dimensional dynamical structure factor is based on the principle of momentum and energy conservation in equation (10). In contrast to indirect geometry instruments it is the incident energy $E_{incident}$ (in cm^{-1}) that is fixed:

$$k_i^2 = \frac{4\pi c E_{incident} m_n}{\hbar} \tag{16}$$

$$k_f^2(\omega) = \frac{4\pi c(E_{incident} - \omega)m_n}{\hbar} \tag{17}$$

Within the proposed model, Θ is the scattering angle with respect to the incident neutron flux. It is assumed that during an experiment neutrons are scattered at many Θ angles. The value of Θ is treated as a free parameter with a range which can be defined by the user. A spectrum for a given atom and quantum order event is obtained as a sum over all spectra for different values of Θ. Also, it is assumed within this model that the resolution function $f(\omega)$ can be represented by a single Gaussian, equation (14), whose width depends on the incident energy selected:

$$\sigma(\omega) = AE_{incident} \tag{18}$$

with A as a constant which depends on the instrumental resolution.

3. Capabilities of AbINS

AbINS is implemented as a Mantid algorithm. and is run from the GUI provided within the Mantid environment, figure 2). The first step is to set the source of the DFT phonon data, this is done by setting the option *DFTprogram*. Currently a user can chose one of two options; *CRYSTAL* or *CASTEP*, in the future AbINS will be extended to support more DFT programs. Once the DFT program is set, the appropriate phonon data is loaded. This is done by setting the *PhononFile* field. Optionally, by selecting the *ExperimentalFile* field, a user can also provide experimental data, which can be compared against modelled data. Currently a user can load only data from indirect geometry instruments, but there are plans to include direct geometry instruments. Next, one can define a temperature in K. Unlike some older implementations, [5], [6] the temperature dependence is fully implemented in the evaluation of the Debye-Waller factors. Temperature dependence of INS spectra are often important to investigate the dynamics of individual atomic species within materials shedding light on the important contributions of those atoms in the mechanism of operation of functional materials [7].

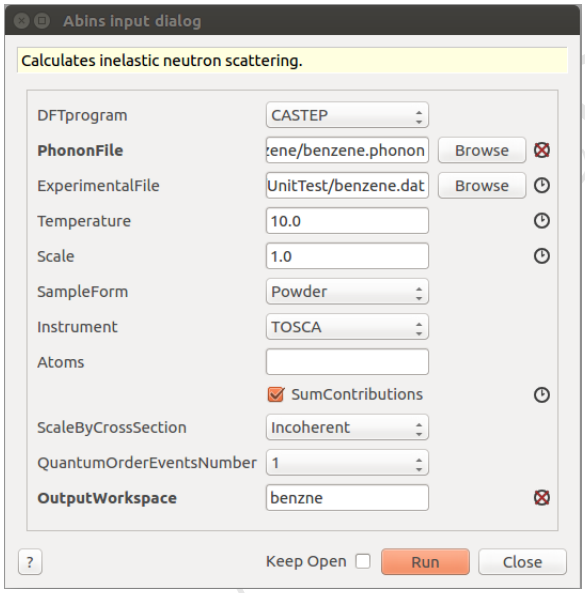

Figure 2: (Colour online) AbINS run in GUI mode.

AbINS produces *S(Q, E)* in scaled units which are related to the correct units barn/cm^{-1} by a linear factor. With CASTEP data, AbINS uses the values of atomic masses read directly from the phonon file. For CRYSTAL, the masses are taken from Mantid because no atomic masses are provided in the CRYSTAl output. The neutron cross sections are taken from Mantid.

In order to better compare the modelled results with experimental data, a user can rescale the theoretical spectrum using the field *Scale*. The form of the sample for which the simulation should be performed is set by *SampleForm*. Currently, only *Powder* option is available but there are plans to implement single crystal simulations. By setting *Atoms*, a user can also define for which type of atom dynamical structure factors are added to the Mantid workspace. For example, if a user would define H, then only the dynamical structure factor for hydrogen atoms would be included in the Mantid workspace. If a user ticks *SumContributions* then the total *S(Q, E)* for the whole system is calculated. A user can also choose which cross sections to use (*ScaleByCrossSection* field). By setting *QuantumOrderEvent* one defines how many quantum order events should be taken into account in the calculation of *S(Q, E)* for each atom. Finally, in order to run calculations, a Mantid workspace is defined in the *OutputWorkspace* field. More detailed documentation of the input parameters can be found in the web documentation [8].

The calculation is started by clicking on the *Run* button. After execution, AbINS saves each workspace to an ASCII file. A user can also save workspaces to one or many Nexus files. The whole project can also be saved in the dedicated Mantid format.

Since Mantid itself can be also used as a library, AbINS can be used inside Python scripts which helps to automate calculations. During its execution AbINS saves all intermediate results to an hdf file so that they can be re-used in the case of a re-run to speed up the calculations.

4. AbINS: benchmarks

The first benchmark is crystalline benzene, (figure 3). AbINS is a *Mantid algorithm* and is invoked like any other Mantid algorithm. Both experiment (from TOSCA [9]) and simulation are at 10 K. Four quantum order events have been included in the calculation of the simulated spectrum and *SumContributions* has been set to true. As a result, several *Mantid workspaces* have been generated for each atom type and each quantum order event respectively. The total simulated spectrum is a summed spectrum over all atomic spectra (both C and H). From figure 3 it can be clearly seen that AbINS produces a simulated spectrum for crystalline benzene which is in good agreement with experiment.

The next benchmark is croconic acid ($C_5H_2O_5$). This is a fascinating organic material, which exhibits above room temperature ferroelectricity in its crystalline form.

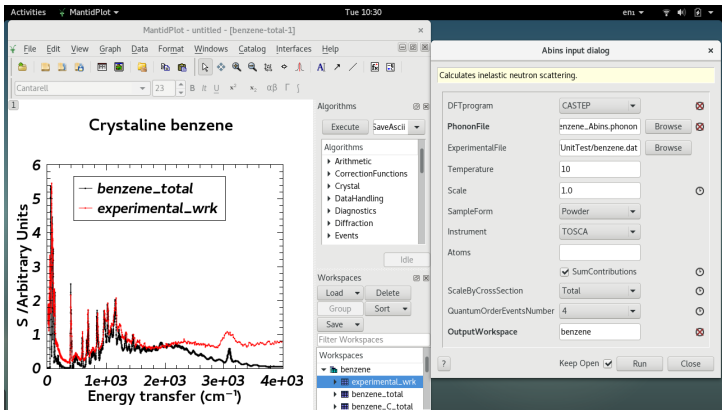

Figure 3: (Colour online) Crystalline benzene: simulated and experimental [10] INS spectra. the screen-shot is from a running instance of Mantid with AbINS. By default, Mantid workspaces with all types of atoms and all quantum events are created. In the case of benzene, atomic type projected workspaces for atoms C and H are created.

Figure 4 shows the total *S(Q, E)* calculated by AbINS (red curve) from a full phonon dispersion calculation *versus* experimental results (black curve) [11]. The calculated INS spectrum agrees well with experiment except for an overall shift in mode frequencies of about 15% relative to experimental values which is consistent with the reported results [11]. The calculated spectrum is in good agreement with previously published data [11], which were produced by aCLIMAX [6].

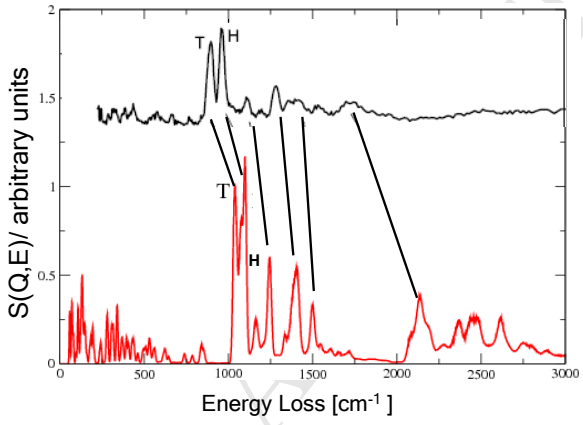

Figure 4: (Colour online) Croconic acid: comparison between theoretical (red curve) and experimental (black curve) [11] at 5 K *S(Q, E)*.

The next system of choice to benchmark AbINS is $CsHSO_4$. This is an interesting material, because at the critical temperature of 141 ^{o}C it becomes a superionic conductor. Its high proton conductivity means that it is considered to be a prime candidate for use in proton exchange membrane fuel cells. The INS spectrum of $CsHSO_4$ in phase III is presented in figure 5. The total *S(Q, E)* calculated by AbINS is the red curve and the experimental *S(Q, E)* [12] is the black curve. The spectrum was recorded with TXFA, which is an older generation of a TOSCA-like instrument. As in the previous examples, the spectrum simulated by AbINS matches the experimental results quite well.

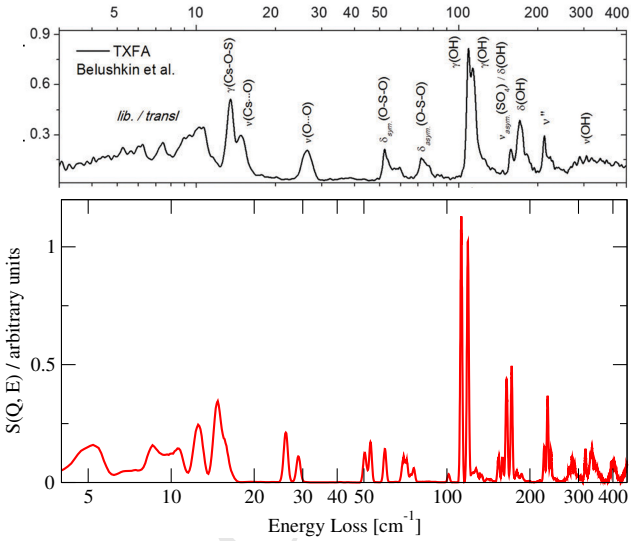

Figure 5: (Colour online) $CsHSO_4$: comparison between calculated (red curve) and experimental [12] (black curve) at 10 K *S(Q, E)*.

The dynamical structure factor calculated by AbINS includes not only fundamentals but also higher order quantum events. How AbINS can decompose the INS spectrum with respect to quantum events is presented in figure 6 (lower panel) for methylammonium lead triiodide ($CH_3NH_3PbI_3$, Mapi). This is one of the most promising light-absorbing materials for solar-energy applications. Again, good agreement with the experimental results (figure 6, upper panel) [13] is obtained.

AbINS is also applicable to non-hydrogenous systems with K_2SiF_6 chosen as an example (figures 7, 8). The INS spectrum of this material has not been previously reported. The complex is cubic, space group (number 225) [14], with the $[SiF_6]^{2-}$ion on the octahedral site and the K^+ ions on tetrahedral sites. Thus there are rigorous selection rules, with the consequence that only some of the modes have been observed by infrared and Raman spectroscopy [15]. The absence of selection rules in INS spectroscopy is a major advantage of the technique [4]. In particular, the T_{1g} librational mode of the $[SiF_6]^{2-}$ ion at 50 cm^{-1} (calculated at 68 cm^{-1}) and the T_{2u} F–Si–F bending mode at 251 cm^{-1} (calculated at 256 cm^{-1}) are detected for the first time. A comparison with aCLIMAX [5] is

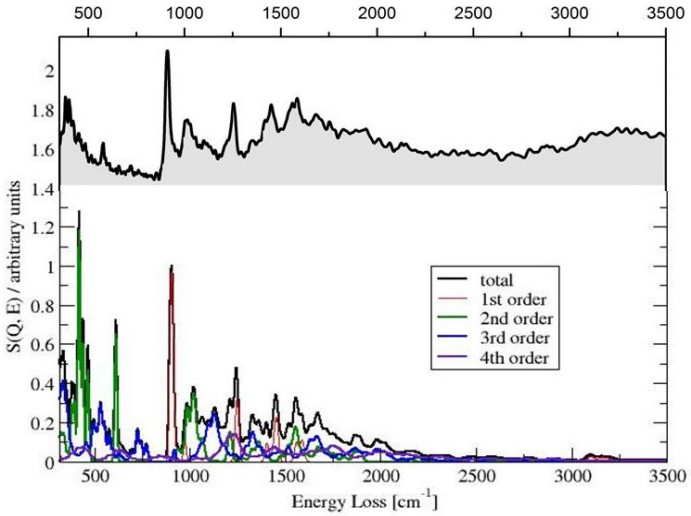

Figure 6: (Colour online) Upper panel: the experimental INS spectrum (curved shape filled with grey) of Mapi [13] at 20 K. Lower panel: total *S(Q, E)* for Mapi obtained by AbINS and its decomposition into different quantum order events.

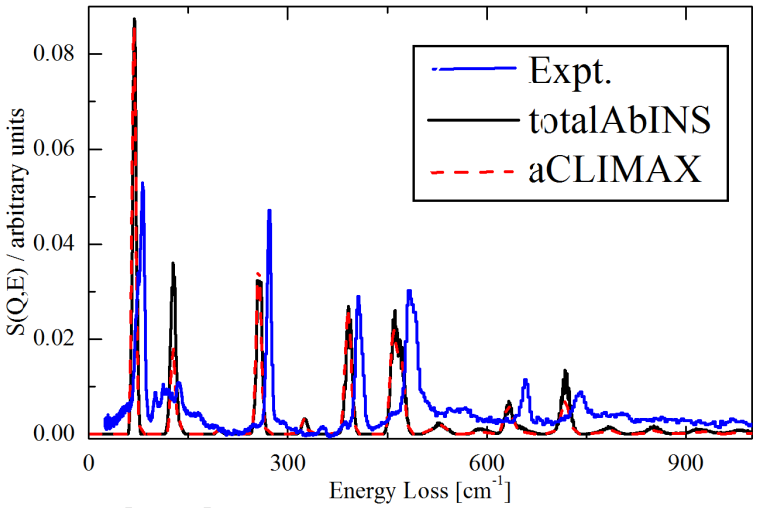

Figure 7: (Colour online) INS spectrum of K_2SiF_6: comparison between AbINS and aCLIMAX with experiments at 10 K.

presented in figure 7. One can observe an almost perfect match between the two calculated spectra. In figure 8 the decomposition of the spectrum into the constituent atom types has been performed by AbINS. As expected, the dynamic structure factor of F, the lightest element in the system, that also has the largest total scattering cross section, dominates the spectrum, as shown by the similarity of the total scattering and the F-only scattering in figure 8. The heaviest elements in the system, Si and K, have only a marginal contribution to spectrum. This straightforward decomposition of S(Q, E) into atom types is one of the strengths of AbINS.

Finally, we show an example of a 2D map calculation, which can be compared against data from direct geometry instruments, (figure 9). The system which has been used in this benchmark is gold acetylide (AuC≡ CH). Since the calculations were performed by the plane wave code CASTEP, the molecule was placed in a large box 10Å×10Å×15Å and the phonon spectrum calculated only at the Γ point. In figure 9 one can see a 2D map of *S(Q, E)* for this model system, which used an incident energy of 4100 cm^{-1}. One can clearly observe a peak at 2200 cm^{-1} which corresponds to the C≡C stretch [16] and a peak at 3300 cm^{-1} which is characteristic of an acetylenic ≡C-H stretch [16]. The whole spectrum presented in figure 9 is a sum of many spectra; one for each angle (3° to 140° in steps of 0.1°). Overall, regardless of the simplicity of the model for direct geometry instruments, the implementation produces useful results.

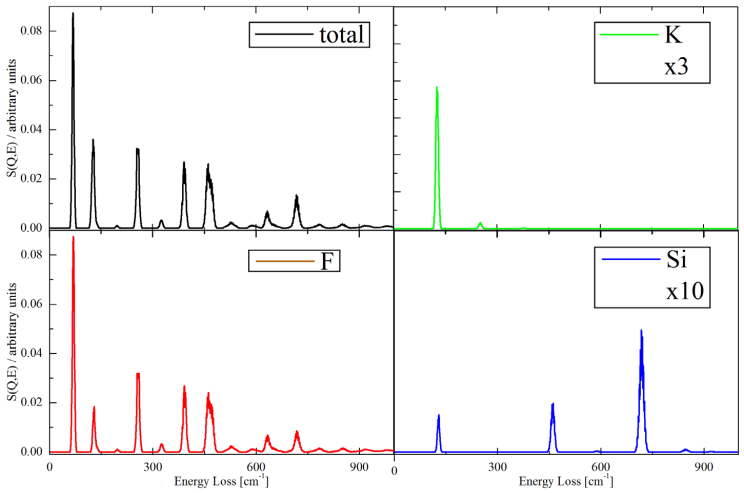

Figure 8: (Colour online) Decomposition of dynamical structure factor into its atom type contributions of INS spectrum of K_2SiF_6

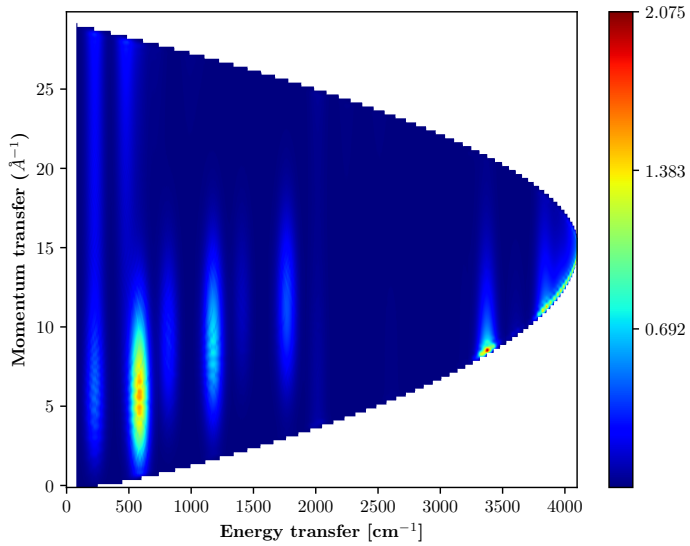

Figure 9: (Colour online) AbINS can produce a 2D map, which can be compared against inelastic neutron scattering data generated by a direct geometry spectrometer. The figure shows 2D *S(Q, E)* for the model system AuC≡CH.

5. Conclusions and future work

In this article we have described a new tool for INS analysis: AbINS. Within the Mantid framework, it is now possible to perform both data reduction of experimental results and comparison with theoretical data. This tool has been applied to analyse the vibrational spectrum of non-hydrogenous K_2SiF_6 for the first time to extract atom-type contributions.

AbINS is in constant development and many new features are scheduled to be added. Firstly, there are plans to add support for more DFT programs. Currently AbINS is written purely in Python, but the intention is to rewrite the most computationally demanding components in C++ to boost performance. Improving performance will provide opportunities to implement more accurate methods of powder averaging, which go beyond those already implemented using the semi-empirical formula [4]. Evaluation of *S(Q, E)* for single crystals is also planned. Direct comparison of experimental *S(Q, E)* from direct geometry instruments with the AbINS result is also intended. A more realistic resolution function for direct geometry instruments is a priority. At present some parameters have to be set outside the program *via* the *AbinsParameters* file. However, it is planned to completely re-write the AbINS GUI using PyQT in such a way that a user will be able to set all parameters from within the GUI.

Acknowledgements The authors thank Kacper Drużbicki and Leonardo Bernasconi for help in preparing the benchmarks mentioned in this document and for their suggestions for improvements and changes. The authors also thank the ISIS Pulsed Neutron and Muon Source for financial support.

References

[1] O. Arnold, J. Bilheux, J. Borreguero, A. Buts, S. Campbell, L. Chapon, M. Doucet, N. Draper, R. F. Leal, M. Gigg, V. Lynch, A. Markvardsen, D. Mikkelson, R. Mikkelson, R. Miller, K. Palmen, P. Parker, G. Passos, T. Perring, P. Peterson, S. Ren, M. Reuter, A. Savici, J. Taylor, R. Taylor, R. Tolchenov, W. Zhou, J. Z. c, Nucl. Instr. Meth. Phys. Res. Sect. A 764 (2014) 156 – 166. doi:10.1016/j.nima.2014.07.029.

[2] S. J. Clark, M. D. Segall, C. J. Pickard, P. J. Hasnip, M. I. J. Probert, K. Refson, M. C. Payne, Zeit. fuer Kristall. 220 (2005) 567 – 570. doi:10.1524/zkri.220.5.567.65075.

[3] R. Dovesi, R. Orlando, A. Erba, C. M. Zicovich-Wilson, B. Civalleri, S. Casassa, M. F. L. Maschi and, M. D. L. Pierre, P. D'Arco, Y. Noël, M. Causà, M. Rérat, B. Kirtman, Int. J. Quant. Chem. 114 (2014) 1287–1317. doi:10.1002/qua.24658.

[4] P. C. H. Mitchell, S. F. Parker, A. J. Ramirez-Cuesta, J. Tomkinson, Vibrational Spectroscopy with Neutrons, World Scientific, 2005.

[5] A. J. Ramirez-Cuesta, Comput. Phys. Commun. 157 (2004) 226–238. doi:10.1016/S0010-4655(03)00520-4.

[6] D. Champion, J. Tomkinson, G. Kearley, Appl. Phys. A 74 (2002) s1302–s1304. doi:10.1007/s003390101223.

[7] S. Mukhopadhyay, M. J. Gutmann, M. Jiménez-Ruiz, D. B. Jochym, K. T. Wikfeldt, K. Refson, F. Fernandez-Alonso, Phys. Chem. Chem. Phys. 19 (2017) 32147–32744. doi:10.1039/c7cp06039d.

[8] http://docs.mantidproject.org/v3.9.1/algorithms/Abins-v1.html.

[9] http://www.isis.stfc.ac.uk/instruments/tosca/tosca4715.html.

[10] H. Jobic, A. N. Fitch, Studies in Surf. Sci. and Catal. 105 (1997) 559–566. doi:10.1016/S0167-2991(97)80601-5.

[11] S. Mukhopadhyay, M. Gutmann, F. Fernandez-Alonso, Chem. Phys. 427 (2013) 95–100. doi:10.1039/c4cp03713h.

[12] M. Krzystyniak, K. Drużbicki, F. Fernandez-Alonso, Phys. Chem. Chem. Phys. 17 (2015) 31287–31296. doi:10.1039/C5CP05636E.

[13] K. Drużbicki, R. S. Pinna, S. Rudić, M. Jura, G. Gorini, F. Fernandez-Alonso, J. Phys. Chem. Lett. 7 (2016) 4701–4709. doi:10.1021/acs.jpclett.6b01822.

[14] J. R. Hester, E. Maslen, N. Spadaccini, N. Ishizawa, Y. Satow, Acta Cryst. B 49 (1993) 967–973. doi:10.1107/S0108768193005725.

[15] R. B. Badachhape, G. Hunter, L. D. McCory, J. L. Margrave, Inorg. Chem. 5 (1966) 929–931. doi:10.1021/ic50039a045.

[16] D. Lin-Vien, N. B. Colthup, W. G. Fateley, J. Grasselli, The Handbook of Infrared and Raman Characteristic Frequencies of Organic Molecules, Academic Press, Boston, 1991.